

Precision measurement of the antiproton-to-proton ratio by the Alpha Magnetic Spectrometer on the International Space Station

Andrew Ian Chen* on behalf of the AMS Collaboration

Massachusetts Institute of Technology

E-mail: achen7@mit.edu

A precision measurement, with the Alpha Magnetic Spectrometer, of the antiproton-to-proton ratio in the primary cosmic rays is presented. The measurement is made in the rigidity range from 1 to 450 GV and is based on 300,000 antiproton events. The measurement increases the precision and significantly extends the high rigidity range beyond previous observations.

*38th International Conference on High Energy Physics
3-10 August 2016
Chicago, USA*

* Speaker

1. Introduction

We report the measurement of the antiproton flux, antiproton-to-proton flux ratio, and properties of elementary particle fluxes in primary cosmic rays (CR) by the Alpha Magnetic Spectrometer (AMS). This measurement published in [1] of the antiproton flux, and of the antiproton-to-proton flux ratio in CR covers the rigidity range of 1 to 450 GV and is based on 3.49×10^5 antiproton events and 2.42×10^9 proton events. The events were collected by AMS aboard the International Space Station (ISS) from May 19, 2011 to May 26, 2015.

The measurement of CR antiprotons (\bar{p}) is complementary to the measurement of CR positrons (e^+) presented in [2,3]. AMS has now measured the properties of all the elementary particles in the cosmos [1,3–5]. This allows for new observations of their properties. The data on e^\pm have already generated many interesting theoretical models. These models will be constrained by further measurements by AMS such as those described in [6].

2. The AMS Detector and Event Selection

To measure the \bar{p} flux to 1% accuracy requires a separation power between \bar{p} and p of $\sim 10^6$. We use all the AMS detector elements [7] for particle identification and selection among the 65 billion CR triggers recorded. The detector elements are: the silicon tracker surrounded by permanent magnet, the time of flight counters (TOF), the anticoincidence counters (ACC), the transition radiation detector (TRD), the ring imaging Čerenkov detector (RICH), and the electromagnetic calorimeter (ECAL).

The nine layer tracker is used to measure the rigidity R (momentum per unit of charge) of CR and to differentiate between positive and negative particles. For particles with absolute charge $|Z| = 1$ the maximum detectable rigidity is 2 TV. CR events are selected with $\chi^2/\text{d.o.f.}$ of the track fit less than 10. Only primary CR are selected by requiring R to be greater than 1.2 times the geomagnetic cutoff.

The TOF measures charge, selects downward-going particles, and measures velocity with a resolution of $\Delta\beta/\beta = 4\%$. The ACC is used to reject CR entering from the side. The TRD separates \bar{p} and p from e^- and e^+ using the Λ_{TRD} estimator constructed from the ratio of the log-likelihood probability of the e^\pm hypothesis to that of the \bar{p} or p hypothesis [3]. The dE/dx measured in the TRD, the TOF, and the tracker are required to be consistent with $|Z| = 1$.

For $|Z| = 1$ the RICH has a velocity resolution $\Delta\beta/\beta = 0.1\%$ which ensures separation of \bar{p} and p from light particles (e^\pm and π^\pm). The separation using the RICH velocity measurement and TRD estimator is show in Figure 1. Light negative mesons are present only at rigidities below 10 GV. Finally, the ECAL is used to separate \bar{p} and p from e^- and e^+ based on shower shape. The ECAL is also used for selecting a pure sample of e^- .

3. Data Analysis

The combination of information from the detector elements enables the efficient separation of the \bar{p} signal from background. This is done using template fitting. The number of observed \bar{p} signal events and its statistical error in each bin is found by fitting signal and background templates to data. The signal template is defined using the high-statistics proton data sample. This is possible because the distribution of the variables for the template definition is the same

for \bar{p} and p if they are both reconstructed with a correct charge-sign. This is done for a detailed Monte Carlo simulation based on the GEANT 4.10.1 package [8]. It has also been verified using \bar{p} and p data for $2.97 \leq |R| < 18.0$ GV.

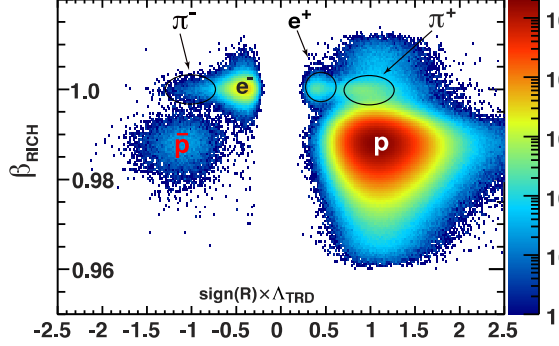


Figure 1: Data samples for the absolute rigidity range 5.4–6.5 GV clearly separated by the RICH and TRD.

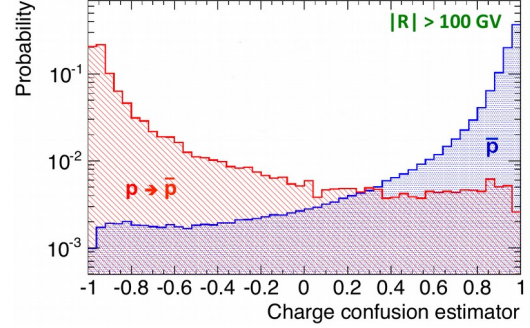


Figure 2: The performance of the charge confusion estimator.

For rigidities above 10 GV, separating \bar{p} from charge confusion p becomes the primary challenge. These are p which are reconstructed with negative rigidity due to the finite tracker resolution. This separation is done using a charge confusion estimator, Λ_{CC} , which is defined using the boosted decision tree technique. The separation power of Λ_{CC} is shown in Figure 2.

The template fit is then done in the two-dimensional, Λ_{TRD} – Λ_{CC} , plane. To fit the data three template shapes are defined: \bar{p} with correctly reconstructed charge sign, e^- , and charge confusion p . The p template is based on the Monte Carlo simulation and verified with p test beam data. An example of the fit for the rigidity bin 175–211 GV is shown in Figure 3. All together there are total of 3.49×10^5 \bar{p} events in the data.

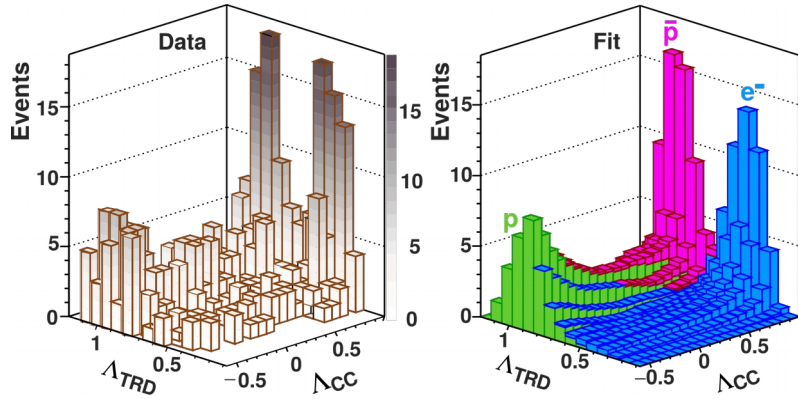


Figure 3: On the left, negative reconstructed rigidity data in the 175–211 GV absolute rigidity bin. On the right, the fit using the \bar{p} signal template, the e^- background template, and the charge confusion p background template. The χ^2 of the fit is 138 for 154 degrees of freedom.

Corrected for bin-to-bin migration using an iterative unfolding technique, we have the number of \bar{p} events at the top of the AMS, $N_i^{\bar{p}}$. This is for a given absolute rigidity bin, R_i . We can then compute the isotropic flux in the bin i with width ΔR_i as

$$\Phi_i^{\bar{p}}(R_i) = \frac{N_i^{\bar{p}}}{A_i^{\bar{p}} T_i \Delta R_i}$$

where $A_i^{\bar{p}}$ is the corresponding effective acceptance including geometric and efficiency effects, and T_i is the exposure time.

4. Systematic Errors

The first source of errors on the \bar{p} flux and (\bar{p}/p) flux ratio are the effects on $N_i^{\bar{p}}$. Variation of the geomagnetic cutoff factor in the range 1.2 to 1.4 shows a systematic uncertainty of $\sim 1\%$ at 1 GV and negligible above 2 GV. The cutoff is calculated by backtracing [5] using the most recent IGRF geomagnetic model [9]. The analysis is also repeated in each rigidity bin with different sets of selections. This resulting uncertainty from event selection amounts to 4% at 1 GV, falls to 0.5% at 10 GV, and rises to a maximum of 6% at 450 GV.

Uncertainties of the proton flux in the TV region are estimated by varying the spectral index of the proton flux within the accuracy of the AMS proton measurement [5]. The systematic errors due to the the shape of the charge confusion proton template originate from uncertainties of the proton rigidity resolution function. They are estimated by comparing the charge confusion predicted by the Monte Carlo simulation with the charge confusion obtained from the fit. The systematic error from these effects are estimated to be to $<1\%$ below 30 GV rising to 12% at 450 GV.

The systematic errors on the folded acceptances, $A_i^{\bar{p}}$ and A_i^p , are attributed to the the uncertainties in the interaction cross sections for protons and antiprotons in the detector materials. This is estimated by varying the \bar{p} and p interaction cross sections in the Monte Carlo simulation. The corresponding error on $A_i^{\bar{p}}$ is found to be 4% at 1 GV and $\sim 1\%$ above 50 GV. The error on A_i^p is found to be 2.5% at 1 GV and $\sim 1\%$ above 50 GV.

The systematic errors from correcting for bin-to-bin migration are 1% below 200 GV and 1.5% at 450 GV. These systematic errors partially cancel in the (\bar{p}/p) flux ratio, yielding uncertainties of 1% at 1 GV and $<0.5\%$ above 2 GV.

The error on the absolute rigidity scale was estimated by comparing the e^\pm energies measured in the ECAL with the momentum measured in the tracker. The corresponding errors on the \bar{p} and p fluxes are negligible below 10 GV and gradually increase to $\sim 1\%$ at 450 GV.

The uncertainty from the Monte Carlo simulation based template shapes are also non-negligible for $|R| > 30$ GV. As reported in [1] and to be detailed separately, these uncertainties

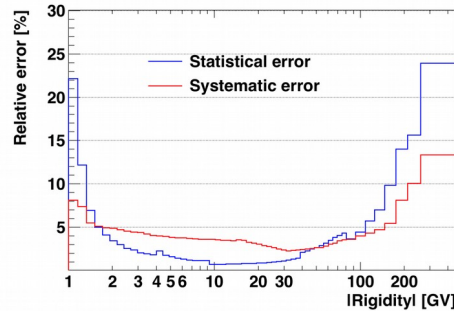


Figure 4: The error breakdown for the (\bar{p}/p) flux ratio.

were verified by a completely independent data driven analysis. This was one of several independent analyses that were performed. The results of these independent analyses are consistent.

The independent sources of systematic error are added together in quadrature to arrive at the total systematic error. The errors on the (\bar{p}/p) flux ratio are shown in Figure 4. At high and low R statistical error dominates. With continued data taking possible through the end of ISS service, AMS will continue to improve this measurement.

6. Results

The measured (\bar{p}/p) flux ratio is presented in Figure 5. A table is available in [1].

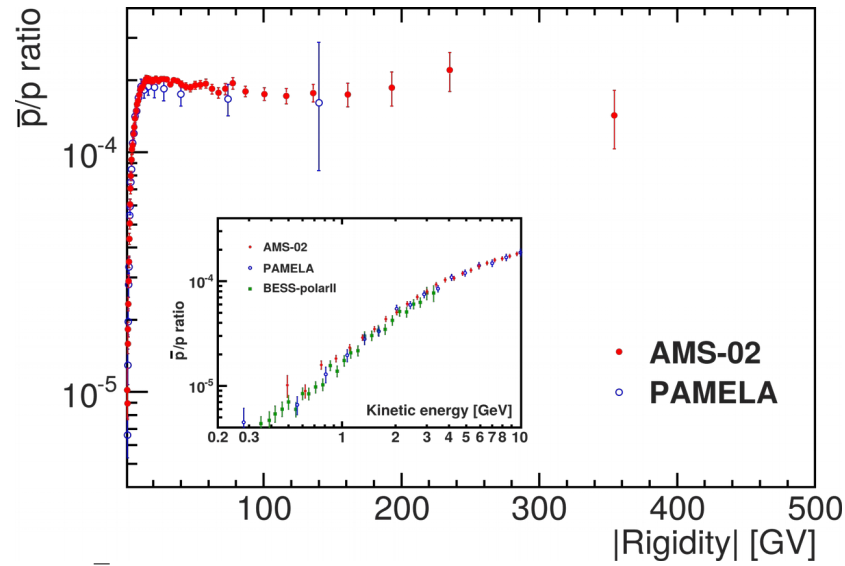


Figure 5: The \bar{p}/p flux ratio as measured by AMS along with previous measurements by BESS [11] and PAMELA [10].

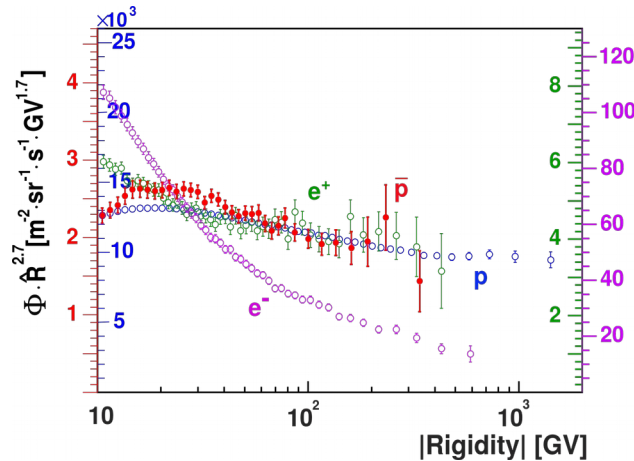


Figure 6: The elementary particle fluxes in primary cosmic rays as measured by AMS.

Compared with earlier experiments [10, 11], the AMS results extend the rigidity range to 450 GV and increase precision. A new observation is that the ratio appears to be rigidity independent at some point. To estimate the lowest rigidity above which the (\bar{p}/p) flux ratio is rigidity independent, we use intervals with varying starting rigidities above 10 GV and ending at the

final bin 450 GV. Each interval is split into two sections. Each of the sections is fit with a constant. The lowest starting rigidity that gives consistent mean values at 90% C.L. defines the lowest rigidity above which the (\bar{p}/p) flux ratio is rigidity independent. This yields 60.3 GV.

AMS has now simultaneously measured the fluxes of e^\pm [4] and of p [5] with a single detector. This enables us to study the overall rigidity dependent behavior of different fluxes as shown in Figure 6. The fluxes for \bar{p} , p , and e^+ show similar rigidity dependence above ~ 60 GV, whereas the rigidity dependence of the e^- flux shows different behavior. Correspondingly, in the absolute rigidity range below 60 GV, the (\bar{p}/p) , (\bar{p}/e^+) , and (p/e^+) flux ratios each reach a maximum. In the absolute rigidity range ~ 60 to ~ 500 GV, the (\bar{p}/p) , (\bar{p}/e^+) , and (p/e^+) flux ratios show no rigidity dependence. These are new observations of the properties of elementary particles in the cosmos.

References

- [1] M. Aguilar *et al.*, *Antiproton Flux, Antiproton-to-Proton Flux Ratio, and Properties of Elementary Particle Fluxes in Primary Cosmic Rays Measured with the Alpha Magnetic Spectrometer on the International Space Station*, *Phys. Rev. Lett.* **117**, 091103 (2016).
- [2] V. Vagelli, *Precision Measurement of the $(e^+ + e^-)$ Flux in Primary Cosmic Rays from 0.5 GeV to 1 TeV with the Alpha Magnetic Spectrometer on the International Space Station*, in proceedings of the 38th International Conference on High Energy Physics **PoS (ICHEP2016) 070**.
- [3] M. Aguilar *et al.*, *First Result from the Alpha Magnetic Spectrometer on the International Space Station: Precision Measurement of the Positron Fraction in Primary Cosmic Rays of 0.5–350 GeV*, *Phys. Rev. Lett.* **110**, 141102 (2013); L. Accardo *et al.*, *High Statistics Measurement of the Positron Fraction in Primary Cosmic Rays of 0.5–500 GeV with the Alpha Magnetic Spectrometer on the International Space Station*, *Phys. Rev. Lett.* **113**, 121101 (2014).
- [4] M. Aguilar *et al.*, *Electron and Positron Fluxes in Primary Cosmic Rays Measured with the Alpha Magnetic Spectrometer on the International Space Station*, *Phys. Rev. Lett.* **113**, 121102 (2014).
- [5] M. Aguilar *et al.*, *Precision Measurement of the Proton Flux in Primary Cosmic Rays from Rigidity 1 GV to 1.8 TV with the Alpha Magnetic Spectrometer on the International Space Station*, *Phys. Rev. Lett.* **114**, 171103 (2015).
- [6] A. Oliva, *Precision Measurement of Boron-to-Carbon and Carbon-to-Helium flux ratio in Cosmic Rays from 2 GV to 2 TV with the Alpha Magnetic Spectrometer on the International Space Station*, in proceedings of the 38th International Conference on High Energy Physics **PoS (ICHEP2016) 072**.
- [7] A. Kounine, *The Alpha Magnetic Spectrometer on the International Space Station*, *Int. J. Mod. Phys. E* **21**, 1230005 (2012)
- [8] S. Agostinelli *et al.*, *GEANT4: A Simulation toolkit*, *Nucl. Instrum. Meth. A* **506** (2003) 250-303.
- [9] E. Thébault *et al.*, *International Geomagnetic Reference Field: the 12th generation*, *Earth Planets Space* **67**, 79 (2015).
- [10] O. Adriani *et al.*, *Measurement of the flux of primary cosmic ray antiprotons with energies of 60 MeV to 350 GeV in the PAMELA experiment*, *JETP Lett.* **96**, 621 (2013).
- [11] K. Yoshimura *et al.*, *Measurement of the Cosmic-Ray Antiproton Spectrum at Solar Minimum with a Long-Duration Balloon Flight over Antarctica*, *Phys. Rev. Lett.* **108**, 051102 (2012).